Structures and molecular dynamics of solution-grown and melt-grown samples of n-hexatriacontane

1994 J. Phys.: Condens. Matter 6 7605

(http://iopscience.iop.org/0953-8984/6/38/003)

J. Phys.: Condens. Matter 6 (1994) 7605–7616. Printed in the UK

Structures and molecular dynamics of solution-grown and melt-grown samples of n-hexatriacontane

E C Reynhardt, J Fenrych and I Basson
Department of Physics, University of South Africa, P O Box 392, Pretoria, 0001, South Africa

Received 13 April 1994, in final form 7 June 1994

Abstract. The crystal structures and molecular dynamics of solution-grown and melt-grown polycrystalline samples of n-hexatriacontane have been investigated by employing NMR, DSC and x-ray powder diffraction techniques. All solution-grown samples have the same orthorhombic structure, while the melt-grown samples are mixtures of a monoclinic and two orthorhombic structures. Defect motions of chain ends between all-*trans* and defect orientations are present in all crystal modifications at room temperature, but defect orientations have significantly higher populations in the orthorhombic structure which occurs only in the melt-grown sample.

1. Introduction

Since the first x-ray studies of n-alkanes were reported by Müller more than six decades ago [1–3], other aspects of these materials have been studied extensively [4–22]. Amongst other things, polymorphism of n-alkanes features prominently in these studies. For example, no less than seven crystal modifications have either been determined or predicted for n-hexatriacontane (C_{36}). Shearer and Vand [7] determined the structure of a monoclinic lattice, while Ohlberg [8] reported three different long spacings for samples which had been recrystallized from the melt. Teare [9] determined the orthorhombic structure (OI) of crystals obtained from a saturated solution of C_{36} in petroleum ether. Sullivan and Weeks [12] observed 00ℓ reflections for an n-alkane sample crystallized from the melt and identified four monoclinic modifications. These polymorphic forms were labelled M_{012}, M_{101}, M_{011} and M_{201}. The latter structure is derived from the OI structure by translating each $-CH_2-$ unit, in the adjacent molecule along the *a* axis, by four $-CH_2-$ units parallel to the *c* axis. The subscript is the Miller subcell index of the plane formed by the terminal methyl groups. Similarly M_{011} may be obtained from the OI unit cell by translating each $-CH_2-$ unit, in the adjacent molecule along the *b* axis, by four $-CH_2-$ units parallel to the *c* axis. Nyburg and Potworowski [13] predicted a triclinic structure which has not yet been observed. Boistelle *et al* [14] and Kobayashi *et al* [15, 16] reported a different orthorhombic structure (OII) consisting of monoclinic layers, one layer being related to the adjacent one by a twofold rotation about the [001] axis. This structure was grown from dilute petroleum ether solutions and is a polytype of the M_{011} structure. The crystallographic parameters of these structures are summarized in table 1.

The main purpose of the present x-ray, NMR and DSC study of C_{36} is to compare the structures, composition, phase transitions and motions of chain ends of solution-grown and melt-grown samples of C_{36}. In addition, the effects of supersaturation and undercooling on the composition of samples have been investigated.

0953-8984/94/387605+12$19.50

Table 1. Cell parameters of the polymorphic forms of C_{36}. Values between parentheses refer to the present study.

Phase	Space group	Z	*a* (Å)	*b* (Å)	*c* (Å)	β (deg)	*V*/chain (Å^3)	Reference
OI	$Pca2_1$	4	7.42	4.96	95.14	90	875	[9]
OII	*Pbcn* or *Pbca*	4	7.40(7.30)	5.58	84.60	90	873	[15]
M_{021}	$P2_1/a$	2	5.12	7.42	48.35	104.4	873	[12]
M_{101}	$P2_1/a$	2	7.84	4.96	48.35	108.9	873	[12]
M_{011}	$P2_1/a$	2	5.57	7.42	48.35	119.1	873	[7]
M_{201}	$P2_1/a$	2	(8.85)	(4.96)	48.35	124.2	875	present study

2. Experimental details

The starting material for all the samples used in this study was a research-grade polycrystalline sample of C_{36} supplied by Fluka. The stated purity of the sample was >99%. Sample A was recrystallized from a saturated solution of C_{36} in C_8 by decreasing the temperature at a rate of ~1.5 K h^{-1} from 318 K to room temperature (294 K). The method of preparation of samples A1, A2 and A3 was similar to that of sample A, except that the temperature was decreased at a very fast rate by immersing the test tube with the saturated solution at 318 K, 340 K and 348 K, respectively, in water at room temperature. All samples were evacuted after preparation.

Two samples were recrystallized from the melt. In both cases the temperature was increased to a few degrees above the melting point and then decreased at a rate of ~5 K min^{-1} (sample B) and ~1 K h^{-1} (sample B1). The preparation methods are summarized in table 3.

All x-ray powder diffractograms were recorded on a Seifert MZ IV diffractometer with Cu Kα radiation and an Ni filter. An accelerating potential of 40 kV, a filament current of 35 mA and detector slits of width 0.01 mm were used.

DSC thermograms were recorded with a Standton Redcroft DSC700 instrument. The samples were heated at a rate of 1 K min^{-1} in open aluminium pans in a nitrogen atmosphere.

Experimental proton second moments, M_2, were obtained as a function of temperature by using a Spin Lock continuous-wave spectrometer operating at 20 MHz. Signal averaging and corrections for finite modulation amplitudes were made on a personal computer interfaced to the spectrometer. The average of up to five spectra was obtained at each temperature. The proton spin-lattice relaxation times in the laboratory frame, T_1, were measured at 75 MHz on a home-made pulse spectrometer by applying a train of sixteen closely spaced 90° saturating pulses, followed at a variable time interval τ by a single 90° measuring pulse. The same saturation method was used in measuring the proton spin-lattice relaxation time in the rotating frame, $T_{1\rho}$, as a function of temperature. In this case the saturating pulse train was followed after about $0.5T_1$ by a 90° RF pulse. This pulse was then followed immediately by a second RF pulse of width τ which was 90° phase shifted with respect to the first pulse. $T_{1\rho}$ values were obtained from the slopes of semi-log plots of magnetization versus τ graphs, where τ was the length of the 90° phase shifted pulse. The relaxation of the magnetization in sample B was found to be slightly non-exponential, but two relaxation times could be isolated from the data only over a relatively narrow temperature region (3 K^{-1} < 1000/T < 4 K^{-1}) by using the equation

$$\frac{M}{M_0} = \left\{ Q \exp\left(\frac{-\tau}{T_{1\rho s}}\right) + (1-Q)\exp\left(\frac{-\tau}{T_{1\rho l}}\right)\right\} \tag{1}$$

where M_0 and M are the magnitization at $t = 0$ and $t = \tau$, respectively. $T_{1\rho s}$ and $T_{1\rho l}$ are the short and long relaxation times, respectively. Q is the fraction of the protons relaxing at the faster rate.

3. Results

The x-ray powder diffractograms for samples A and B, covering the 2θ ranges 3° to 9° and 20° to 26°, are shown as a function of increasing temperature in figures 1 and 2, respectively. The d spacings associated with some of the diffraction peaks are plotted as a function of temperature in figure 3.

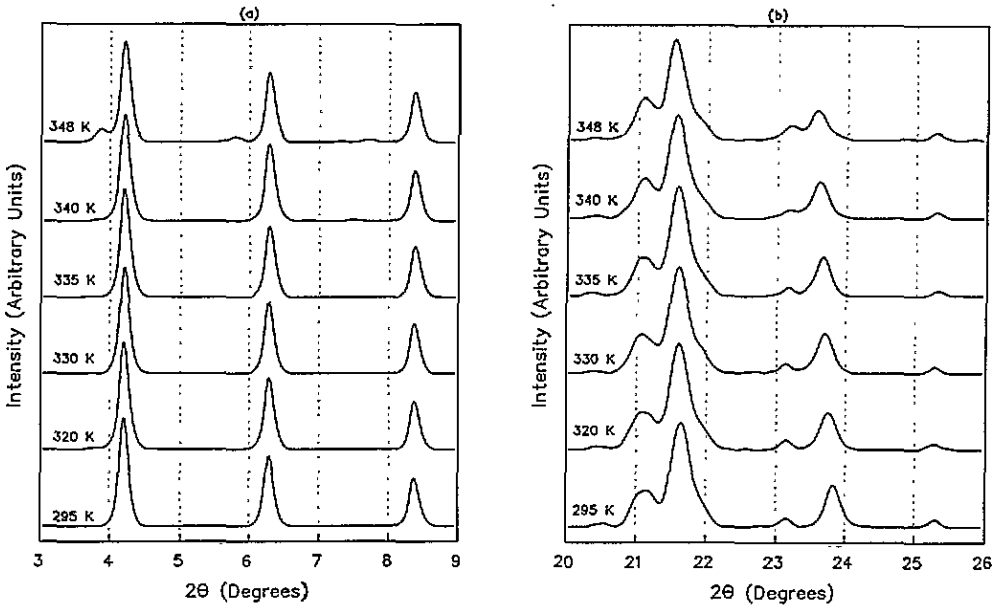

Figure 1. Observed diffractograms for the solution-grown sample A as a function of temperature.

Using the cell parameters listed in table 1, the published atomic coordinates [7, 9, 14–16] and the powder diffraction program RIETVELD [23, 24], diffractograms of the known crystallographic modifications of C_{36} were simulated. These diffractograms are shown in figure 4 for the same 2θ ranges shown in figures 1 and 2.

The DSC thermograms are shown in figure 5. Sample A has a solid–solid transition at ~347 K and a melting *trans*ition at ~349 K. The shoulder on the low-temperature side of this transition was also observed by Takamizawa *et al* [25] and attributed to a transformation to the rotator phase through an intermediate phase. Sample B exhibits two solid–solid transitions at ~337 K and ~350 K. The former transition is relatively weak.

The temperature dependences of T_1 for samples A and B are similar, both reaching a minimum of ~0.4 s in the vicinity of 150 K (figure 6), but the curve for sample A is shifted towards lower temperatures. $T_{1\rho}$ for sample A, shown in the same figure, reaches a minimum of ~13 ms at $\beta \simeq 3.2\ \mathrm{K}^{-1}$, where $\beta = 1000/T$. In the region $3.0\ \mathrm{K}^{-1} < \beta < 4.0\ \mathrm{K}^{-1}$ two

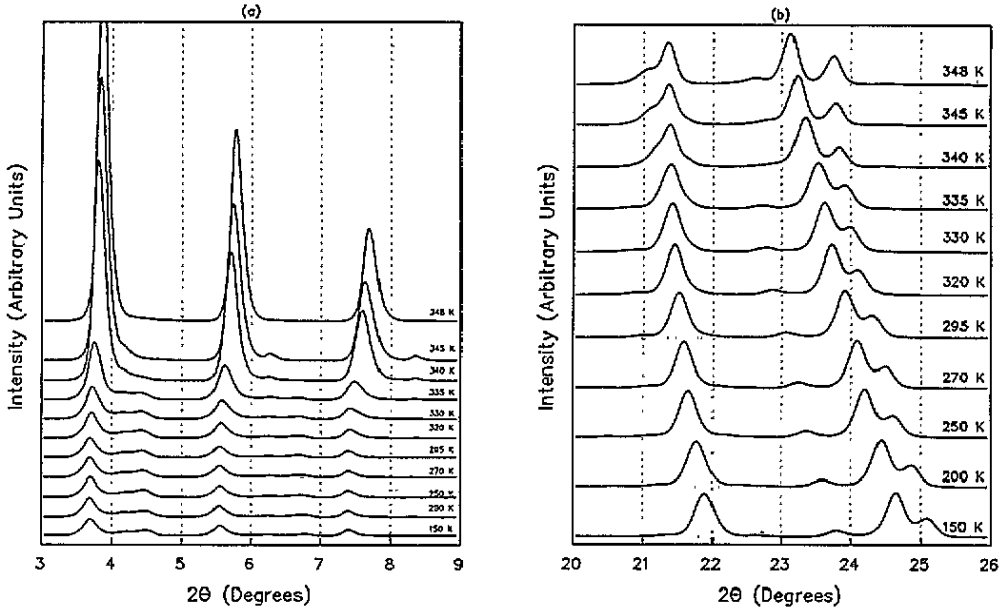

Figure 2. Observed diffractograms for the melt-grown sample B as a function of temperature.

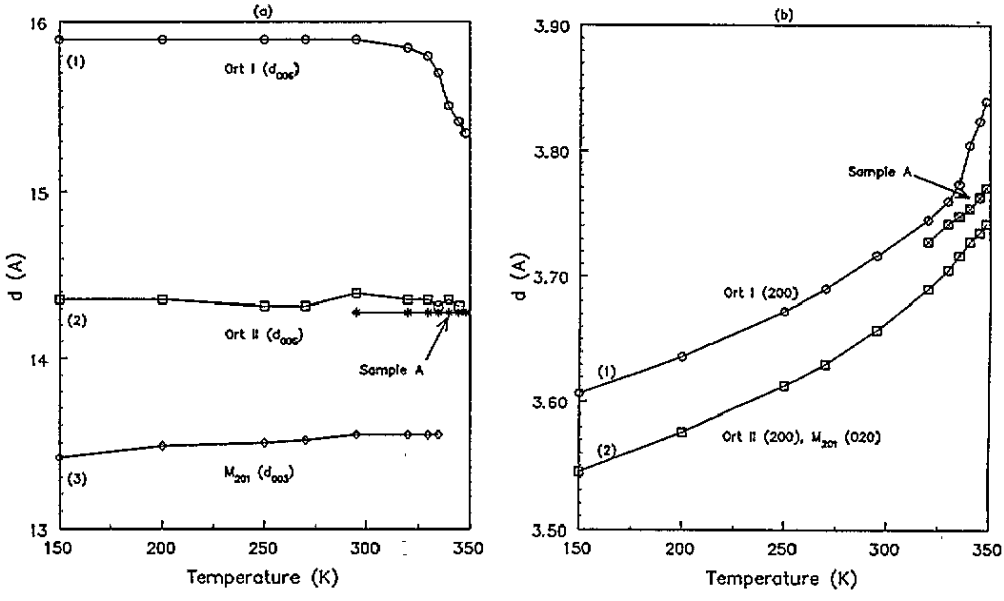

Figure 3. Temperature dependence of a number of selected d spacings.

relaxation times were obtained for sample B. The minimum of the longer relaxation time coincides with that of sample A, while the minimum of the shorter relaxation time is more than a factor of two deeper. In the vicinity of $\beta = 4.2\ \mathrm{K}^{-1}$ $T_{1\rho}$ for sample B is noticeably shorter than that for sample A. This deviation is most probably due to the fact that two

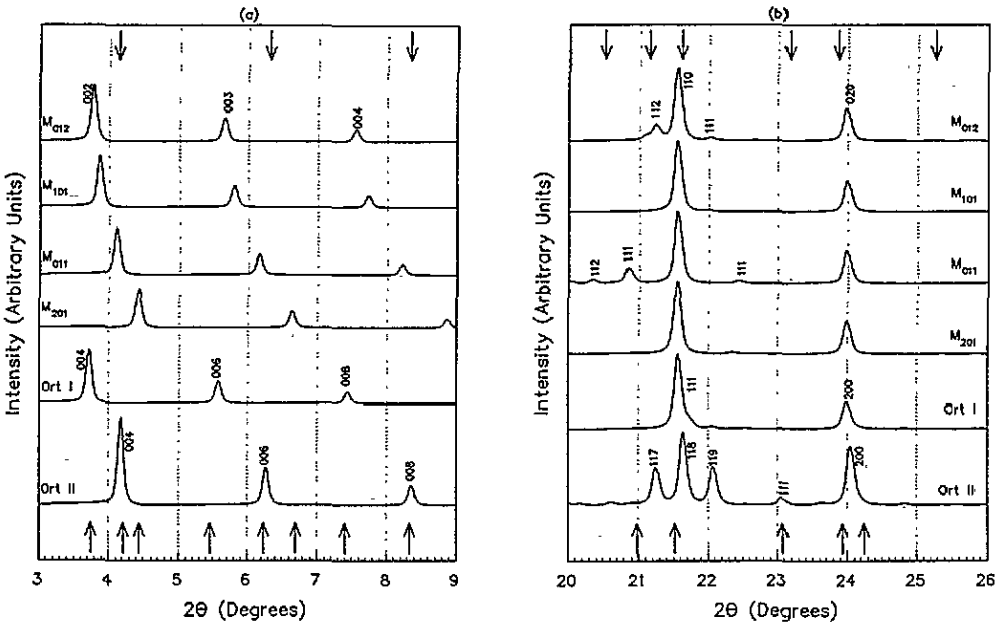

Figure 4. Simulated diffractograms for the different crystal modifications of C_{36}. Arrows at the top of the diagrams indicate observed diffraction peak positions for the solution-grown sample A, while arrows at the bottom indicate diffraction peak positions for the melt-grown sample B.

relaxation times could not be isolated and therefore the single observed relaxation time lies somewhere between the true long and short relaxation times.

The proton second moments for samples A and B are shown as a function of temperature in figure 7. For both samples M_2 remains constant at ~28 G^2 (1 G = 10^{-4} T), the calculated value for rigid chains and reorienting methyl groups, between 150 K and 240 K. Above 340 K M_2 drops sharply to a value compatible with that of a liquid. Between 240 K and 340 K M_2 for sample B is noticeably smaller than for sample A.

4. Discussion

4.1. Identification of the polymorphic structures

The observed diffraction peak positions for samples A and B are indicated by arrows in figure 4. A comparison of these peak positions with the simulated diffractograms, shown in this figure, reveals that sample A has the OII structure.

From the low-angle diffractogram of sample B (figure 2) it is clear that after melting and recrystallization, at least three different long spacings are present. A mixture of OI, OII and M_{201} explains all the features of the observed low-angle diffractogram at room temperature. The agreement between the simulated diffraction peaks of these structures and the observed high-angle diffractogram is satisfactory. The only difference occurs in the region of 24° where the observed splitting of the 200 orthorhombic and 020 monoclinic peaks is larger than predicted by the simulations.

The temperature dependence of the 006 and 200 peaks of the OI structure is shown in figure 3. The c cell dimension at room temperature is in excellent agreement with

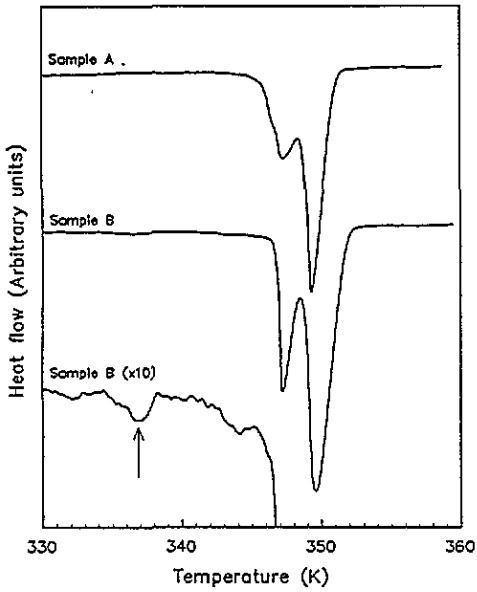

Figure 5. DSC thermograms of solution-grown sample A and melt-grown sample B.

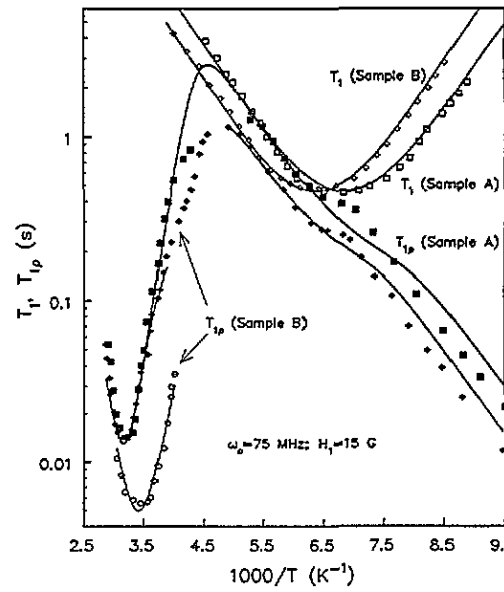

Figure 6. Spin–lattice relaxation times in the laboratory and rotating frames as a function of inverse temperature. Solid lines are best fits of equations (2) and (4) to the experimental data.

the published value c = 95.2 Å [9] for the OI structure. The NMR results, which are discussed in the next section, show that the sharp decrease of c and the sharp increase of a with increasing temperature are related to jump motions of chain ends between all-*trans* and defect orientations. With increasing temperature defect orientations become more populated, resulting in the shortening of the c cell dimension and the lengthening of the a cell dimension to create more space in the ab plane. The observed c cell dimension of 85.2 Å for the OII structure at room temperature agrees well with the reported value of 84.6 Å [15]. The c cell dimension is within experimental uncertainty independent of temperature, implying that defect motions play a less prominent role in this structure. The a cell dimension will also be less temperature dependent than that of OI. The peak at ~24.3° (shorter a axis) is therefore assigned to the 200 reflection of the OII structure. This peak does not show the drastic shift towards lower 2θ angles with increasing temperature observed for the 200 peak of the OI structure. The d_{003} spacing of the M_{201} structure is equivalent to a long spacing of 40.5 Å, in close agreement with the value predicted by Sullivan and Weeks [12]. This spacing is also independent of temperature and most probably the 200 peak of this structure coincides with that of the OII structure. The cell dimensions obtained from the present study are included in table 1.

The calculated diffraction profile for a mixture of OI, OII and M_{201} was fitted to the experimental diffractogram at 294 K between 3° and 9° by treating the relative fractions of the three phases as variable parameters. It was found that ~37% of sample B consists of OI, while OII and M_{201} contribute ~8% and ~55%, respectively.

4.2. Molecular dynamics

The proton T_1 minima of samples A and B are associated with threefold reorientations of

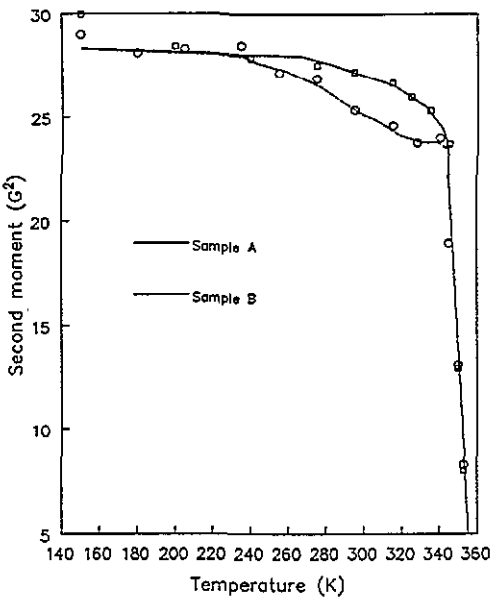

Figure 7. Proton second moments as a function of temperature.

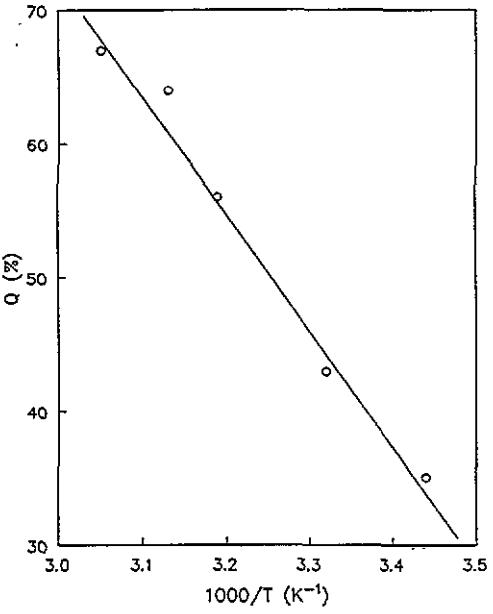

Figure 8. Fraction of protons in the melt-grown sample B relaxing at the faster rate as a function of inverse temperature.

methyl groups. The relaxation rate for such reorientations is given by [26]

$$T_1^{-1} = \tfrac{2}{3}\gamma^2 \Delta M_2 \left(\frac{\tau_c}{1+\omega_0^2\tau_c^2} + \frac{4\tau_c}{1+4\omega_0^2\tau_c^2} \right) \tag{2}$$

where

$$\tau_c = \tau_0 \exp(E/RT) \tag{3}$$

and ω_0 and ΔM_2 are the proton resonant frequency and the proton second moment reduction, respectively.

Table 2. Motional parameters associated with some of the phases of C_{36}.

Sample	Structure	Motion	E (kJ mol^{-1})	ΔE (kJ mol^{-1})	τ_0 (s)	ΔM_2 (G^2)
Solution grown	OII	methyl	10.0±0.5	—	$(3.5\pm0.2)\times10^{-13}$	1.5±0.2
(A)		defect	46±3	7.6±1.0	$(3.5\pm0.2)\times10^{-14}$	
Melt grown	OI	methyl	11.0±0.5	—	$(4.5\pm0.2)\times10^{-13}$	1.5±0.2
(B)		defect	36±5	4.9±1.0	$(6.2\pm0.2)\times10^{-13}$	
	M_{201}	methyl	11.0±0.5	—	$(4.5\pm0.2)\times10^{-13}$	1.5±0.2
		defect	46±3	7.6±1.0	$(3.5\pm0.2)\times10^{-14}$	

Best fits of (2) to the experimental data are shown as solid lines in figure 6. It is clear from the motional parameters listed in table 2 that the threefold motion of methyl groups is slightly less restricted in the solution-grown OII sample than in the melt-grown sample. The second-moment reductions of 1.5±0.2 G^2 obtained from the fits are in agreement with the calculated values of 1.34 G^2 for an isolated methyl group.

The $T_{1\rho}$ results for both samples can be divided into two regions as far as molecular motions are concerned. For $\beta > 4.5\ K^{-1}$ the dominant relaxation mechanism is the threefold reorientations of methyl groups, while at higher temperatures defect motions of chain ends are the major mechanism modulating the dipolar interactions. Basson and Reynhardt [19] have shown that chain ends of n-alkanes ($22 \leqslant n \leqslant 41$) jump between all-*trans* and *gauche* defect orientations at temperatures even below the transition to the rotator phase. The potential minimum for the all-*trans* orientation is lower than that of the defect orientation, the energy difference being ΔE and the barrier height E. For this system the spin-lattice relaxation rate in the rotating frame is given by [27]

$$T_{1\rho}^{-1} = \gamma^2 \Delta M_2 \frac{4a}{(1+a)^2}\left(\frac{\tau_c}{1+4\omega_1^2\tau_c^2} + \frac{5}{3}\frac{\tau_c}{1+\omega_0^2\tau_c^2} + \frac{2}{3}\frac{\tau_c}{1+4\omega_0^2\tau_c^2}\right) \tag{4}$$

where ω_1 is the rotating field strength and

$$a = \exp(\Delta E/RT). \tag{5}$$

Here ΔM_2 is the second moment reduction if $\Delta E = 0$. For C_{36} such a jump motion between an all-*trans* and a single defect orientation at each end of the chain yields $\Delta M_2 \simeq 1\ G^2$. The probability that a chain is in the defect orientation is given by

$$p = \frac{1}{1+a}. \tag{6}$$

The best fit of (4) to the $T_{1\rho}$ data for sample A is shown as a solid line in figure 6. The energy difference $\Delta E \simeq 7.6\ kJ\ mol^{-1}$ is in close agreement with values obtained for other n-alkanes [19]. From (6) it follows that defect orientations are occupied ~25% of the time at 340 K.

Since sample B is a mixture of three polymorphic structures, the protons in each of the structures form a separate spin system. Therefore, the magnetization could relax at three distinct rates. However, since a relatively small fraction of the sample is in the OII phase (~8%), it is assumed that only the relaxation rates of the OI (~40%) and M_{201} (~60%) phases were obtained from the measurements.

Figure 8 shows the temperature dependence of Q in (1) over the limited temperature range where the two components could be isolated with confidence. For this system of two non-interacting spin systems, Q is the fraction of the sample relaxing at the faster rate (shorter relaxation time). From the figure it follows that ~40% of the protons in the sample relax at the faster rate in the vicinity of room temperature, which agrees well with the estimated fraction of the sample belonging to the OI phase. The longer relaxation time is therefore associated with the M_{201} phase.

As explained above, the two relaxation components could not be isolated in the region $\beta > 4.0\ K^{-1}$ for sample B and the measured values in figure 6 were obtained by fitting

one term of (1) to the data. The deviation of the relaxation curve for sample B from that of sample A in the vicinity of $\beta = 3.6\ K^{-1}$ is ascribed to this method of obtaining the relaxation times from the data. Fits of equation (4) to the two sets of relaxation data therefore excluded this temperature region. The motional parameters obtained from these fits are listed in table 2.

The proton spin systems in the OII (sample A) and M_{201} (sample B) structures relax at the same rate in the region where defect motions are effective in influencing $T_{1\rho}$. This result is to be expected since chain packing in the layers of the OII structure and the M_{201} structure is similar.

The sharp decrease in the c cell dimension of the OI phase of sample B is due to the presence of a number of highly populated defect orientations near the chain ends. The corresponding increase in the a cell dimension is attributed to the extra space required by the defects in that direction. For defect motions in this phase $\Delta E \simeq 4.9\ kJ\ mol^{-1}$. From (6) it follows that defect orientations are occupied for ~40% of the time at 340 K, implying that the populations of the defect and all-*trans* orientations are almost equal.

The temperature dependence of the proton second moments (figure 7) confirms the interpretation of the x-ray and spin-lattice relaxation results. The lower second moment of sample B above room temperature is due to the higher jump rate between all-*trans* and defect orientations in the OI structure, resulting in a more effective reduction of the proton second moment [27].

4.3. Crystallization kinetics

With a view to obtaining some information about the effect of the cooling rate on the composition of the samples, the cooling rate for samples crystallized from the melt and from solution was varied, as described earlier (table 3).

Table 3. Preparation methods and composition of C_{36} samples.

Sample	Method	Initial temperature (K)	Cooling rate	Composition
A	Solution grown	318	~1.5 K h^{-1}	OII (100%)
A1	Solution grown	318	>20 K min^{-1}	OII (90%) OI (10%)
A2	Solution grown	340	>20 K min^{-1}	OII (100%)
A3	Solution grown	348	>20 K min^{-1}	OII (100%)
B	Melt grown	350	~5 K min^{-1}	OI (37%) OII (8%) M_{201} (55%)
B1	Melt grown	350	~1 K h^{-1}	OI (39%) OII (49%) M_{201} (12%)

The diffractograms of samples A1, A2 and A3 (fast-cooled saturated solutions) show that these solution-grown samples, like the slow-cooled sample A, consist of only one phase, viz. OII. The only exception is sample A1, which contains a small fraction of OI. Therefore, it seems that supersaturation, with C_8 as a solvent, does not play an important role in the sample composition.

On the other hand the composition of the melt-grown samples is strongly dependent on the cooling rate. A comparison of the diffractograms of samples B and B1, shown in figure 9 for the lower 2θ range, shows that the fraction of the samples which is in the OI

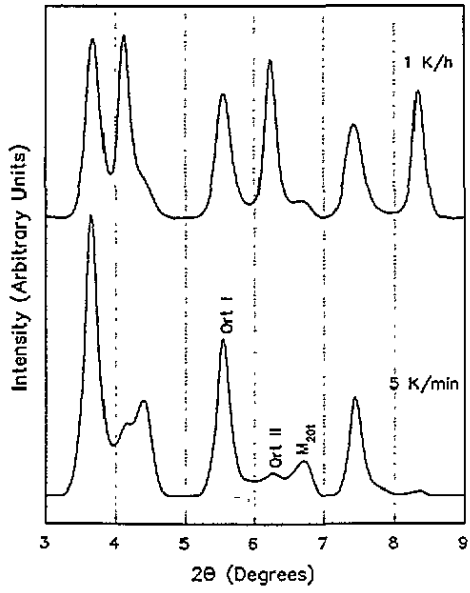

Figure 9. Diffractograms for samples grown from the melt at different cooling rates. Sample B, bottom trace; sample B1, top trace.

phase remains almost constant. However, a lower cooling rate results in a dramatic increase in the OII fraction of the sample at the expense of the M_{201} fraction. The reason for this behaviour is not clear, but the possibility that one of the samples was supercooled cannot be ignored.

4.4. Phase transitions

Figure 2 shows that the M_{201} phase of sample B disappears in the vicinity of 340 K. The temperature dependence of Q (figure 8) also reveals that the fraction of protons belonging to the M_{201} phase decreases with increasing temperature above 250 K. This is the temperature region in which defect orientations are populated up to 25% of the time in this phase. As the defect orientations become more populated, the M_{201} structure transforms gradually to the OI structure. The weak DSC transition at 337 K could be the transition of what is left of the M_{201} modification to the OI structure. It is therefore expected that the 00ℓ peaks of the OI structure should grow in intensity with increasing temperature above room temperature, in agreement with the observed diffractograms shown in figure 2. Sullivan and Weeks [12] also observed an increase in the intensities of the 00ℓ diffraction peaks in a sample similar to sample B and attributed the phenomenon to the thermal expansion of the interlamellar region and thermally generated vacancies, e.g. via kink formation. It has already been shown that kink defects are indeed created in the temperature region under consideration in the OI structure. It is concluded that these factors and the expansion of the OI phase at the expense of the M_{201} phase jointly contribute to the increase in intensity of the OI structure at higher temperatures.

It is well known that n-alkanes transform into a rotator phase a few degrees below the melting point. Ungar [28] showed that shorter n-alkanes, such as C_{23} and C_{25}, reach perfect hexagonal symmetry in this phase. However, recent work by Ungar and Masic [29], Dorset *et al* [30–32] and Sirota *et al* [22] revealed that a number of phase transitions can

occur within the rotator phase and that in some of these phases the chain packing results in distorted hexagonal lattices. In the rotator phases the chains rotate about their long axes and defect orientations are heavily populated [17–19]. The x-ray diffractograms for C_{36} show that at 348 K neither sample A nor sample B is hexagonal, but the sharp reduction of the proton second moment at high temperatures suggests that the chains rotate about their long axes. This behaviour could be explained by the observations of the above-mentioned researchers.

5. Conclusions

The monoclinic structures and the OII structure, which is a polytype of the M_{011} monoclinic structure, have lower total energies than the OI structure. If crystallization takes place from a saturated solution, the OII structure is formed. If crystallization takes place from the melt, the chain ends are mostly in defect orientations and the OI structure with the higher total energy grows faster than the monoclinic structures which favour straight chains. If the temperature of a melt-grown sample is increased, defect orientations are introduced and the monoclinic structures transform to the OI structure. The OI structure is metastable and should transform to OII or the monoclinic structure with the lowest energy as a function of time at room temperature. Ohlberg [8] found that a melt-grown sample of C_{36} still showed polymorphism after a few years, but one of the phases had grown relative to the others.

References

[1] Müller A 1928 *Proc. R. Soc.* A **120** 437
[2] Müller A 1930 *Proc. R. Soc.* A **127** 417
[3] Müller A 1932 *Proc. R. Soc.* A **138** 514
[4] Hoffmann J D 1952 *J. Chem. Phys.* **20** 541
[5] Smith A E 1953 *J. Chem. Phys.* **21** 2229
[6] Schaerer A A, Busso C J, Smith A E and Skinner L B 1955 *J. Am. Chem. Soc.* **77** 2017
[7] Shearer H M M and Vand V 1956 *Acta Crystallogr.* **9** 379
[8] Ohlberg S M 1959 *J. Phys. Chem.* **63** 248
[9] Teare P W 1959 *Acta Crystallogr.* **12** 294
[10] Broadhurst M G 1962 *J. Res. NBS* A **66** 241
[11] McClure D W 1968 *J. Chem. Phys.* **49** 1830
[12] Sullivan P K and Weeks J J 1970 *J. Res. NBS* A **74** 203
[13] Nyburg S C and Potworowski J A 1973 *Acta Crystallogr.* B **29** 347
[14] Boistelle R, Simon B and Pepe G 1976 *Acta Crystallogr.* B **32** 1240
[15] Kobayashi M, Kobayashi T, Itoh Y, Chatani Y and H Tadokoro 1980 *J. Chem. Phys.* **72** 2024
[16] Kobayashi M, Sakagami K and Tadokoro H 1983 *J. Chem. Phys.* **78** 6391
[17] Maroncelli M, Strauss H L and Snyder R G 1985 *J. Chem. Phys.* **82** 2811
[18] Kim Y, Strauss H L and Snyder R G 1989 *J. Phys. Chem.* **93** 7520
[19] Basson I and Reynhardt E C 1990 *J. Chem. Phys.* **93** 3604
[20] Sirota E B, Singer D M and King H E Jr 1994 *J. Chem. Phys.* **100** 1542
[21] Sirota E B, King H E Jr, Huyskens S J and Wan W K 1992 *Phys. Rev. Lett.* **68** 492
[22] Sirota E B, King H E Jr, Singer D M and Shao H H 1993 *J. Chem. Phys.* **98** 5809
[23] Rietveld H M 1969 *J. Appl. Crystallogr.* **2** 5
[24] Schneider J 1987 *Acta Crystallogr.* A **43** Supplement C 295
[25] Takamizawa K, Ogawa Y and Oyama T 1982 *Polym. J.* **14** 441
[26] Kubo R and Tomita K 1954 *J. Phys. Soc. Japan* **9** 888
[27] Andrew E R and Latanowicz L 1986 *J. Magn. Reson.* **68** 232
[28] Ungar G 1983 *J. Phys. Chem.* **87** 689
[29] Ungar G and Masic N 1985 *J. Phys. Chem.* **89** 1036

[30] Dorset D L, Hu H and Jäger J 1991 *Acta Crystallogr.* A 47 543
[31] Dorset D L 1990 *EMSA Bull.* 20 54
[32] Dorset D L, Moss B, Wittmann J C and Lotz B 1984 *Proc. Natl Acad. Sci.* 81 1913